Generating High-Current Monoenergetic Proton Beams by a Circularly Polarized Laser Pulse in the Phase-Stable Acceleration Regime

X. Q. Yan(颜学庆),[1,5,*] C. Lin(林晨),[1] Z. M. Sheng(盛政明),[1,2,3] Z. Y. Guo(郭之虞),[1] B. C. Liu(刘必成),[1,4]
Y. R. Lu(陆元荣),[1] J. X. Fang(方家驯),[1] and J. E. Chen(陈佳洱)[1]

[1]*State Key Laboratory of Nuclear Physics and Technology, Institute of Heavy Ion Physics, Peking University, Beijing 100871, China*
[2]*Beijing National Laboratory for Condensed Matter Physics, Institute of Physics, CAS, Beijing 100080, China*
[3]*Department of Physics, Shanghai Jiao Tong University, Shanghai 200240, China*
[4]*The Graduate University of Chinese Academy of Science, Beijing, China*
[5]*Center for Applied Physics and Technology, Peking University, Beijing 100871, China*

(Received 24 October 2007; published 3 April 2008)

A new ion acceleration method, namely, phase-stable acceleration, using circularly-polarized laser pulses is proposed. When the initial target density n_0 and thickness D satisfy $a_L \sim (n_0/n_c)D/\lambda_L$ and $D > l_s$ with a_L, λ_L, l_s, and n_c the normalized laser amplitude, the laser wavelength in vacuum, the plasma skin depth, and the critical density of the incident laser pulse, respectively, a quasiequilibrium for the electrons is established by the light pressure and the space charge electrostatic field at the interacting front of the laser pulse. The ions within the skin depth of the laser pulse are synchronously accelerated and bunched by the electrostatic field, and thereby a high-intensity monoenergetic proton beam can be generated. The proton dynamics is investigated analytically and the results are verified by one- and two-dimensional particle-in-cell simulations.

DOI: 10.1103/PhysRevLett.100.135003 PACS numbers: 52.38.Kd, 41.75.Jv, 52.35.Mw, 52.59.−f

State-of-the-art lasers can deliver ultraintense, ultrashort laser pulses with very high contrast ratios. These systems can avoid plasma formation by the prepulse, and can thus realize laser-matter interaction with ultrathin solid targets [1]. Solid targets irradiated by a short pulse laser can be an efficient and flexible source of MeV protons. They have already been used in producing high-energy-density matter [2], radiographing transient processes [3], tumor therapy [4], generating isotopes in positron emission tomography [5], and fast ignition of fusion cores [6].

In intense-laser interaction with solid foils, there are usually three groups of accelerated ions. The first two occur at the front surface, moving backward and forward, respectively [7–9], and the third is the target normal sheath acceleration (TNSA) that occurs at the rear surface [10,11]. As these output beams are accelerated only by the electrostatic fields and have no longitudinal bunching in the laser direction, their distributions are exponential with nearly 100% energy spread. Certain techniques can be used to decrease the energy spread [12], but they rely on relatively complicated target fabrication.

In the surface acceleration mechanisms, a linear polarized (LP) laser pulse is normally used and the $J \times B$ heating [13] generates hot electrons. For a circularly polarized (CP) laser pulse with the electrical field $E_L = E(x)[\sin(\omega_L t)\hat{y} + \cos(\omega_L t)\hat{z}]$, the ponderomotive force $\vec{f}_p = -\frac{m_e c^2}{4}\frac{\partial}{\partial x}a_L^2(x)\hat{x}$ has no oscillating component. Here, $a_L(x) = eE/m_e\omega_L c$ is the normalized laser amplitude, and m_e, ω_L, and e are the electron mass, laser frequency, and charge, respectively. When a CP laser is normally incident on a thin foil, the electrons are pushed forward steadily by the ponderomotive force. Using this feature, Shen *et al.* [14] proposed to use two CP laser pulses to compress deuterium plasma for inertial-confinement fusion (ICF) studies, Macchi *et al.* [15] found that high-current proton beams are generated by a CP laser. Ion bunching and acceleration were not noticed in these studies. In this Letter, we show that in the interaction of a CP laser with a thin foil there is a regime of proton acceleration in which the proton beam is synchronously accelerated and bunched like in a conventional radio frequency (RF) linac [16]. The acceleration mechanism is referred to as phase-stable acceleration (PSA). An analytic model is presented, showing the acceleration and bunching processes duration the laser interaction.

At first we carried out simulations using a fully relativistic one-dimensional (1D) particle-in-cell (PIC) code [17]. In our simulation a laser pulse with a peak amplitude $a_L = 5$ and the duration $100T_L$ is normally incident on a plasma slab, where T_L is a laser period. To simplify the model, a low density purely hydrogen plasma with a step density profile is used (the initial normalized density $n_0/n_c = 10$ and thickness $D = 0.2\lambda_L$). The target boundary is located at $x = 10\lambda_L$ and the laser front impinges on it at $t = 10T_L$. We take $100 \sim 500$ particles per species per cell and the cell size of $\lambda_L/100$.

Figure 1(a) shows the snapshots of the electrostatic field profile. Because of the ponderomotive push, the electrons are quickly piled up in the front of the CP laser pulse and an electron depletion region is left behind. The depletion region increases with time, so that the ion density is decreased in the debunching process. In the compressed electron layer, it is found that the width of the layer remains equal to the skin depth ($l_s \cong \lambda_L/20$). The charge separa-

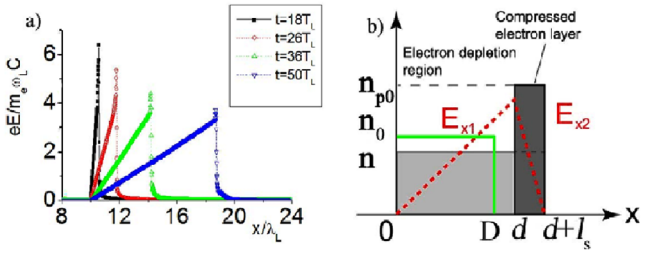

FIG. 1 (color online). (a) Snapshots of the spatial distribution of the electrostatic field at different times, for initial plasma density $n_0/n_c = 10$, thickness $D = 0.2\lambda_L$, normalized laser amplitude $a_L = 5$, and pulse duration $100T_L$, (b) Schematic of the equilibrium density profiles for ions (n) and electrons (n_{p0}). The position at $x = d$ indicates the electron front, where the laser evanescence starts and it vanishes at $x = d + l_s$, where l_s is the plasma skin depth. The initial plasma density n_0 and target thickness D are also plotted.

tion field in this layer retains nearly the same steep linear profile. Therefore a simple 1D model can be used [see Fig. 1(b)]. The induced electrostatic fields have linear profiles both in the depletion region ($E_{x1} = E_0 x/d$ for $0 < x < d$) and in the compression layer ($E_{x2} = E_0[1 - (x - d)/l_s]$ for $d < x < d + l_s$). The parameters E_0, and n_{p0} are l_s related by $E_0 = 4\pi end$ and $n_{p0} l_s = nd \approx n_0 D$. The light pressure $(1 + \eta) I_L/c$ (with η is the reflecting efficiency) exerted on the electrons is assumed to be balanced by $E_0 e n_{p0} l_s/2$, the electrostatic pressure in the depleted region. Usually one has $D \geq l_s$, so that the balance condition can be expressed as

$$a_L(1 + \eta)^{1/2} \sim (n_0/n_c)(D/\lambda_L). \tag{1}$$

To obtain this expression, we have taken $I_L \lambda_L^2 = \pi P_0 a_L^2 = [2.74 \times 10^{18}\ \mathrm{W/cm^2}\ \mu\mathrm{m}^2] a_L^2$ with $P_0 = m_e^2 c^5/e^2 = 8.67$ GW [18]. If the laser field E_L is larger than the maximum charge separation field $E_\parallel$, all electrons will be displaced, then no balance exists. Accordingly, we have the second condition for PSA: $E_\parallel = 4\pi e n_0 D > (v_e \times B_L/c) \sim E_L$ or

$$a_L < (n_0/n_c)(2\pi D/\lambda_L). \tag{2}$$

The steep profile of the electrostatic field E_{x2} remains until the laser pulse is over [see Fig. 1(a)]. This provides a longitudinal restoring force for the ions in the compressed electron layer. Just like PSA in the conventional RF Linac, when a proper synchronous phase is chosen the early ions experience a smaller field, and the later ions a larger field than the synchronous particle, which is kept in synchronization with the accelerating field. As the ions execute longitudinal oscillations under the restoring field E_{x2}, we introduce a reference particle to explain the phase motion. The reference particle is assumed to remain in synchronization with the compressed electron layer, which moves at a high speed under the ponderomotive force.

In order to describe the interaction between the ions and the electron layer, we now derive the ion dynamic equations. We introduce $\xi = (x_i - x_r)$ with $-l_s/2 \leq \xi \leq l_s/2$, where $x_r = d + l_s/2$ represents the position for the reference ion and x_i, the position for the test ion inside the electron layer. The force acting on the test ion is given by $F_i = q_i E_0[1 - (x_i - d)/l_s]$. Thus, the equation of motion for the ion is $\frac{d(m_i \gamma_i \dot{x}_i)}{dt} = q_i E_0[1 - (x_i - d)/l]$ or $\frac{d^2 x_i}{dt^2} = \frac{q_i E_0}{m_i \gamma_i^3}[1 - (x_i - d)/l_s]$, where γ_i is the relativistic factor for the reference particle. The phase motion (ξ, t) around the reference particle can be described approximately by

$$\ddot{\xi} = -\Omega^2 \xi, \qquad \Omega^2 = \frac{q_i E_0}{m_i l_s \gamma_i^3}, \tag{3}$$

where it is assumed that $\gamma_i \approx \gamma_r$. Furthermore, if both γ_i and E_0 vary slowly in a time scale of $1/\Omega$, then the longitudinal phase motion (ξ, t) is a harmonic oscillation $\xi = \xi_0 \sin(\Omega t)$. The beam energy spread can be estimated from $\dot{\xi} = \xi_0 \Omega \cos(\Omega t)$ and $\Delta w/w_r \cong 2\Delta p/p_r \cong 2\xi_0 \Omega/p_r$, where w_r and p_r are the kinetic energy and momentum of the reference particle, respectively, and ξ_0 is the oscillating amplitude. An ion located at $\xi < -l_s/2$ will be debunched and lost in the acceleration process. Some ions are rapidly accelerated by the electrostatic shock and can overrun the electron layer, but they will get no more energy until they return to the electron layer. Accordingly, the particle displacement in the oscillation is $\xi_{\max} \leq l_s/2$ and the maximum energy spread of the accelerated beam is determined by $\Delta w/w_r \cong l_s \Omega/p_r$. The harmonic oscillation frequency Ω decreases with increase of particle energy. For the simulation parameters given in Fig. 1(a) with $a_L = 5$, $n_0/n_c = 10$, and $\gamma_i = 1$ for the proton, the first period of phase oscillation is about $8T_L$ and the period will lengthen as long as E_0 and $1/\gamma_i$ are decreased. If the final energy of the reference particle $w_r = 300$ MeV, the estimated energy spread $\Delta w/w_r$ will be less than 5%. These agree very well with the results of our PIC simulations.

Snapshots of phase-space distributions of electrons and ions at $t = 200T_L$ are given in Figs. 2(a) and 2(b). A bunched proton beam of very high density is formed in the phase space (x, p_x). This is because the protons inside the compressed electron layer always execute periodical oscillations as described by Eq. (3). The protons in the electron depletion region (between $x = 0$ and 100) are debunched and form a long tail in the phase space. However, its density is two orders lower than that in the compressed electron layer. As a result, the debunched protons appear to have disappeared in the proton spatial distribution and energy spectrum, as shown in Figs. 2(c) and 2(d), respectively. Figure 2(c) shows that both particles have the same density profiles and a quasineutral beam is therefore formed. In this case, the space charge field is weak and the proton beam can propagate over a long

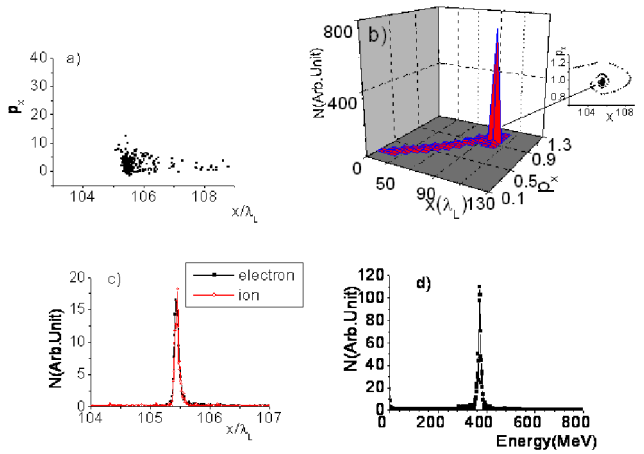

FIG. 2 (color online). (a) Phase-space distribution of electrons, (b) phase-space distribution of protons, (c) electron and proton density profiles, (d) energy spectrum of protons. The results are for $t = 200T_L$ when the laser interaction is almost terminated. The laser and plasma parameters are the same as in Fig. 1.

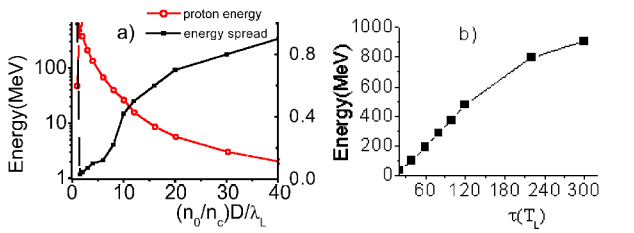

FIG. 3 (color online). (a) Proton energy of the monoenergetic peak versus target thickness and density for $a_L = 5$ and $\tau = 100T_L$, (b) proton energy of the monoenergetic peak versus laser pulse duration for $a_L = 5$, $n_0/n_c = 10$, and $D = 0.2\lambda_L$.

distance without explosion, which is advantageous in applications for the transport of the high-current ion beams. The energetic proton beam has a low-FWHM-energy spread (<4%) and high peak current, as shown in Fig. 2(d). The energy spread is in complete agreement with our analytical estimate based on Eq. (3). Note that the proton bunch has an ultrashort scale length of about the skin depth l_s or about 250 asec ($\lambda_L = 800$ nm) in time. The number of accelerated protons in the bunch is about $n_0 l_s \sigma$, where σ is the focused beam spot area. This gives about 5×10^{12} quasi-monoenergetic protons for a focused beam diameter of 40 μm in the present simulation.

It is found that the reflection coefficient of the incident laser is about $\eta = 0.38$, which implies that more than 60% of the laser energy is converted into the electron and proton energy. The simple model of a flat foil in Ref. [19] is used to explain the high conversion efficiency. The accelerated foil, which consists of the electron and ion layers, can be regarded as a relativistic plasma mirror copropagating with the laser pulse. The plasma mirror acquires an energy $(1 - 1/4\gamma^2)\varepsilon_L$ from the laser pulse. Figure 2(d) shows that the relativistic factor γ of the plasma mirror reaches about 1.4, which implies a conversion efficiency of above 80%. This is overestimated since the plasma mirror does not reach such a high speed in the earlier stage of the laser interaction.

In the 1D simulation it is found that the proton energy depends on the product of target density and thickness. This is similar to the results of Ref. [10] in spite of a different acceleration mechanism. The proton energy and the energy spread are plotted versus the electron area density in Fig. 3(a). It shows that the energy spread can be optimized near $a_L \sim (n_0/n_c)D/\lambda_L$. If the target is thinner than the skin depth of the laser pulse, the latter can transmit through the target and the light pressure is less efficient to push the electrons. The maximum proton energy occurs at about 3 times the normal skin depth due to relativistic effects [20]. For example, in order to get the energetic proton beam needed for fast-ignition in inertial confined fusion [6], one may use a laser driver with wavelength $\lambda_L \cong 0.351$ μm ($n_c = 0.9 \times 10^{22}$ cm^{-3}), intensity $a_L = 5$ and a plastic-foil (CH_2) with thickness $D = 0.5\lambda_L$. In this case a density of $n_0 \cong 10^{23}$ cm^{-3} would satisfy the PSA condition. Figure 3(b) suggests that at first the proton energy increases almost linearly with the laser pulse duration, later it is saturated as the protons become relativistic [19].

The results obtained so far are based upon the 1D model. However, real experiments are always multidimensional. We performed 2D simulations, which indicate that the PSA mechanism is also effective. The incoming laser pulse has a rise time of $2T_L$ and a Gaussian radial profile with half-width $5\lambda_L$, pulse duration $\tau = 50T_L$, $a_L = 5$ and $D = 0.1\lambda_L$ (the plasma density rises linearly from 0 to n_0/n_c in a distance of $0.05\lambda_L$). The density is $n_0/n_c = 100$ and the ions are protons. Although the energy spectrum is broadened due to the transverse laser profile, the monoenergetic peak is fairly consistent with that from the 1D simulations [about 7 MeV shown in Fig. 4(a)]. As lasers with a transverse profile can bend the plasma surface [Fig. 4(b)], the quasi-monoenergetic peak becomes broadened. Furthermore, the $J \times B$ heating of electrons becomes important while the plasma slab is curved as shown in Fig. 4(c). The fast electrons can go backward and forward through the plasma slab and lead to TNSA. Surface accelerations enhance the energy gain of protons and further increase the energy spread. Since the protons inside the compressed electron layer are bunched by the electrostatic field, the output beam is still quasineutral, like in 1D case as shown in Figs. 4(b). The backward ion acceleration can be seen in the proton angular distribution plotted in Fig. 4(d), which shows that the maximum divergence angle of the forward-moving particles is less than 15° and the relative spread of the transverse momentum $\sqrt{\langle p_y^2 \rangle / \langle p_x^2 \rangle}$ is about 0.08, suggesting that the acceleration is perpen-

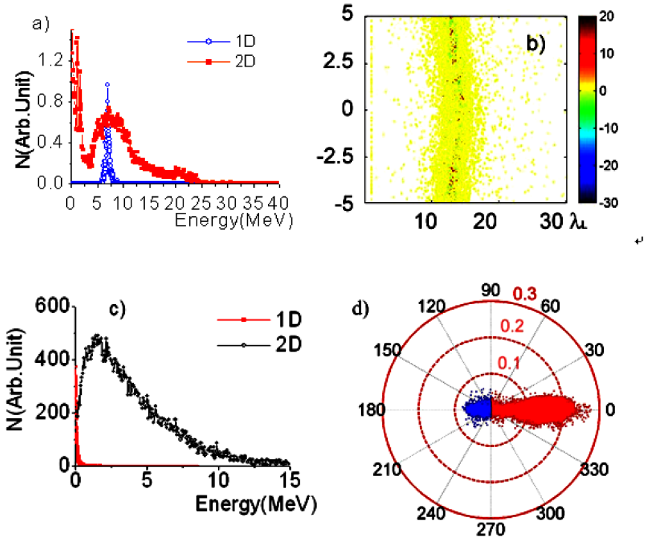

FIG. 4 (color online). (a) Energy spectrum of protons, (b) spatial distribution of $n_e - n_i$, (c) energy spectrum of electrons, (d) angular distribution of proton energy, where the blue and red dots represent the backward and forward particles, respectively, and the radial circles are labeled in red for the normalized momentum). All the above results are obtained at $t = 65T_L$.

dicular to the target surface and the output beam is highly collimated.

From the simulations, we can conclude that higher current and monoenergetic and collimated proton beam can be realized in the realistic multidimensional geometry. Even though the laser profile tends to bend the plasma surface and in some runs results in hole boring [15], and Rayleigh-Taylor and Weibel-like instabilities appear, these factors increase the energy spread and limit the higher energy gain. The larger laser spot size will be helpful to mitigate the hole boring effects and instabilities.

In conclusion, a new mechanism of proton acceleration, namely, the PSA, has been proposed. A simple analytical model for the evolution of the accelerated protons is given, and the results are verified by 1D and 2D PIC simulations. When the condition $a_L \sim (n_0/n_c)D/\lambda_L$ is satisfied, the protons are synchronously accelerated and bunched like that in a radio frequency accelerator, therefore high-current and monoenergetic proton beams can be generated with a high laser-to-ions energy conversion efficiency. A simple analytical model for proton acceleration in this new regime is given, and the results are verified by 1D and 2D PIC simulations.

We acknowledge helpful discussions with Dr. Yutong Li, Dr. Min Chen at IOP, CAS and Professor Z. Z. Xu, Professor Yu Wei, Professor Baifei Shen at SIOM, CAS and Dr. Wei Lu at UCLA. This work was supported in part by NSFC (under Grant No. 10455001, No. 10605003, No. 10425416, No. 10674175), the National High-Tech ICF Committee in China, and National Basic Research Program of China (Grant No. 2007CB815105).

*X.Yan@pku.edu.cn

[1] A. J. Mackinnon *et al.*, Phys. Rev. Lett. **88**, 215006 (2002).
[2] P. Patel *et al.*, Phys. Rev. Lett. **91**, 125004 (2003).
[3] M. Borghesi *et al.*, Phys. Plasmas **9**, 2214 (2002).
[4] S. V. Bulanov, T. Zh. Esirkepov, V. S. Khoroshkov, A. V. Kuznetsov, and F. Pegoraro, Phys. Lett. A **299**, 240 (2002).
[5] I. Spencer *et al.*, Nucl. Instrum. Methods Phys. Res., Sect. B **183**, 449 (2001).
[6] M. Roth *et al.*, Phys. Rev. Lett. **86**, 436 (2001).
[7] E. L. Clark *et al.*, Phys. Rev. Lett. **85**, 1654 (2000); A. Zhidkov *et al.*, Phys. Rev. E **60**, 3273 (1999).
[8] J. Denavit, Phys. Rev. Lett. **69**, 3052 (1992).
[9] A. Zhidkov, M. Uesaka, A. Sasaki, and H. Daido, Phys. Rev. Lett. **89**, 215002 (2002); L. O. Silva, M. Marti, J. R. Davies, R. A. Fonseca, C. Ren, F. Tsung, and W. B. Mori, Phys. Rev. Lett. **92**, 015002 (2004); A. Maksimchuk, S. Gu, K. Flippo, D. Umstadter, and V. Y. Bychenkov, Phys. Rev. Lett. **84**, 4108 (2000).
[10] P. Mora, Phys. Rev. Lett. **90**, 185002 (2003); T. Esirkepov, M. Yamagiwa, and T. Tajima, Phys. Rev. Lett. **96**, 105001 (2006).
[11] Y. T. Li and Z. M. Sheng *et al.*, Phys. Rev. E **72**, 066404 (2005).
[12] H. Schwoerer *et al.*, Nature (London) **439**, 445 (2006); B. M. Hegelich *et al.*, Nature (London) **439**, 441 (2006).
[13] W. L. Kruer *et al.*, Phys. Fluids **28**, 430 (1985).
[14] B. F. Shen and J. Meyer-ter-Vehn, Phys. Plasmas **8**, 1003 (2001); Phys. Rev. E **65**, 016405 (2001).
[15] A. Macchi, F. Cattani, T. V. Liseykina, and F. Cornolti, Phys. Rev. Lett. **94**, 165003 (2005).
[16] T. P. Wangler, *Principles of RF Linear Accelerators* (John Wiley & Sons Inc, New York, 1998), p. 172.
[17] Z.-M. Sheng *et al.*, Phys. Rev. Lett. **85**, 5340 (2000).
[18] J. Meyer-ter-Vehn, A. Pukhov, and Z.-M. Sheng, in *Atoms, Solids, and Plasmas in Super-Intense Laser Fields*, edited by D. Batani *et al.* (Kluwer Academic/Plenum, Dordrecht, 2001), p. 167.
[19] T. Esirkepov, M. Borghesi, S. V. Bulanov, G. Mourou, and T. Tajima, Phys. Rev. Lett. **92**, 175003 (2004).
[20] Q.-L. Dong, Z.-M. Sheng, M. Y. Yu, and J. Zhang, Phys. Rev. E **68**, 026408 (2003).